

27 **Abstract**

28 The cloud condensation nuclei (CCN) properties of atmospheric aerosols were measured on
29 May 1-30, 2011 at the HKUST Supersite, a coastal site in Hong Kong. Size-resolved CCN
30 activation curves, the ratio of number concentration of CCN (N_{CCN}) to aerosol concentration
31 (N_{CN}) as a function of particle size, were obtained at supersaturation (SS) = 0.15%, 0.35%, 0.50%,
32 and 0.70% using a DMT CCN counter (CCNc) and a TSI scanning mobility particle sizer
33 (SMPS). The mean bulk size-integrated N_{CCN} ranged from $\sim 500 \text{ cm}^{-3}$ at $SS = 0.15\%$ to ~ 2100
34 cm^{-3} at $SS = 0.70\%$, and the mean bulk N_{CCN}/N_{CN} ratio ranged from 0.16 at $SS = 0.15\%$ to 0.65 at
35 $SS = 0.70\%$. The average critical mobility diameters (D_{50}) at $SS = 0.15\%$, 0.35%, 0.50%, and
36 0.70% were 116 nm, 67 nm, 56 nm, and 46 nm, respectively. The corresponding average
37 hygroscopic parameters (κ_{CCN}) were 0.39, 0.36, 0.31, and 0.28. The decrease in κ_{CCN} can be
38 attributed to the increase in organic to inorganic volume ratio as particle size decreases, as
39 measured by an Aerodyne high resolution time-of-flight aerosol mass spectrometer (HR-ToF-
40 AMS). The κ_{CCN} correlates reasonably well with κ_{AMS_SR} based on size-resolved AMS
41 measurements: $\kappa_{AMS_SR} = \kappa_{org} \times f_{org} + \kappa_{inorg} \times f_{inorg}$, where f_{org} and f_{inorg} are the organic and inorganic
42 volume fractions, respectively, $\kappa_{org} = 0.1$ and $\kappa_{inorg} = 0.6$, with a R^2 of 0.51.

43 In closure analysis, N_{CCN} was estimated by integrating the measured size-resolved N_{CN} for
44 particles larger than D_{50} derived from κ assuming internal mixing state. Estimates using κ_{AMS_SR}
45 show that the measured and predicted N_{CCN} were generally within 10% of each other at all four
46 SS . The deviation increased to 26% when κ_{AMS} was calculated from bulk PM1 AMS
47 measurements of particles because PM1 was dominated by particles of 200 nm to 500 nm in
48 diameter, which had a larger inorganic fraction than those of D_{50} (particle diameter < 200 nm).
49 A constant $\kappa = 0.33$ (the average value of κ_{AMS_SR} over the course of campaign) was found to
50 give an N_{CCN} prediction within 12% of the actual measured values. We also compared N_{CCN}
51 estimates based on the measured average D_{50} and the average size-resolved CCN activation
52 ratio to examine the relative importance of hygroscopicity and mixing state. N_{CCN} appears to be
53 relatively more sensitive to the mixing state and hygroscopicity at a high $SS = 0.70\%$ and a low
54 $SS = 0.15\%$, respectively.

55 1 Introduction

56 Atmospheric aerosols can act as cloud condensation nuclei (CCN) and affect cloud
57 formation by influencing the CCN number concentration (N_{CCN}) and the size of cloud droplets.
58 Whether aerosol particles will eventually form cloud droplets under a set atmospheric condition
59 mainly depends on their size, chemical composition, and mixing states. Predicting N_{CCN} usually
60 involves measuring the aerosol size distribution and making assumptions about the chemical
61 composition associated to mixing state. Bulk chemical compositions and an assumption of
62 internal mixing state (i.e., particles are identical mixtures of all participating species) are often
63 used in predicting N_{CCN} (Moore et al., 2012a; Wang et al., 2010). Ambient aerosols are complex
64 mixtures and the aerosol compositions vary substantially with particle size. The hygroscopicity
65 parameter (κ) is used to represent the effect of chemical composition on CCN activity (Petters
66 and Kreidenweis, 2007, 2013). Size-resolved chemical compositions give a size-dependent κ
67 which leads to better N_{CCN} predictions than those based on bulk compositions (Medina et al.,
68 2007; Stroud et al., 2007; Wang et al., 2010).

69 While the real-time aerosol size-resolved chemical compositions such as non-refractory
70 (NR)-species and black carbon (BC) can be obtained with an aerosol mass spectrometer and a
71 single particle soot photometer, respectively, information on the mixing state is usually not
72 available or incomplete. Various assumptions have been applied to describe the aerosol mixing
73 state (Asa-Awuku et al., 2011; Bougiatioti et al., 2009; Cubison et al., 2008; Ervens et al., 2010;
74 Lance et al., 2009; Latham et al., 2013; Moore et al., 2012a; Rose et al., 2011; Wang et al.,
75 2010). N_{CCN} predictions assuming internal mixing are usually larger than measured values by 20%
76 or even more, since this assumption overestimates the contribution of organics to N_{CCN} (Rose et
77 al., 2011; Wang et al., 2010; Wex et al., 2010). Another extreme assumption is external mixing,
78 which is when the aerosol contains different types of particles but each particle consists of a
79 single species (Textor et al., 2006; Zhang et al., 2010). Under this assumption, the number
80 concentration (N_{CN}) of each type of particles is determined as the product of the total N_{CN} and
81 the volume fraction of the species. The D_{50} of a species is calculated based on its κ (Moore et al.,
82 2012a; Wang et al., 2010) and N_{CCN} is obtained by integrating N_{CN} above D_{50} . Finally, the total
83 N_{CCN} is calculated by adding up all the predicted N_{CCN} of the species. This simplified external

84 mixing state assumption could underestimate N_{CCN} . For example, Wang et al. (2010) reported
85 an underestimation of ~20% in N_{CCN} at supersaturation (SS) from 0.11% to 0.35%. Aerosol
86 mixing state and chemical composition are thus important factors that need to be considered in
87 the CCN prediction, especially in places where anthropogenic aerosol emission is strong and
88 pollution is heavy (Ervens et al., 2010; Kammermann et al., 2010; Kerminen et al., 2012; Rose
89 et al., 2010; Wang et al., 2010).

90 Recently, measurements of the condensation nuclei (CN) and CCN spectra simultaneously
91 by combining a scanning mobility particle sizer (SMPS) and a CCN counter (CCNc) have been
92 made (Asa-Awuku et al., 2010; Lance et al., 2009; Moore et al., 2012a; Moore et al., 2010;
93 Padró et al., 2010; Rose et al., 2010). The size-resolved CCN activation ratios, i.e., the fraction
94 of the measured N_{CCN}/N_{CN} as a function of particle size, are the combined results of the size
95 distribution, size resolved chemical composition, and the mixing state of the aerosols. Deng et
96 al. (2013) estimated N_{CCN} by integrating the product of the measured size-distributed N_{CN} and
97 the averaged size-resolved CCN activation ratio at each particle size bin measured at Wuqing in
98 the North China Plain. The estimated and measured values differed by less than 6% at $SS = 0.06\%$
99 to 0.81%.

100 In recent years, the rapid urbanization and industrial development in the Pearl River Delta
101 (PRD) have resulted in heavy air pollution, especially particulate matter (PM) pollution (Chan
102 and Yao, 2008). Hong Kong, a typical coastal city south-east of the PRD, is affected by PM due
103 to both local anthropogenic emissions and transportation of pollutants from the PRD (Li et al.,
104 2014).

105 In this study, we report for the first time size-resolved measurements of CCN activity in
106 Hong Kong. We correlated the CCN-derived hygroscopicity (κ_{CCN}) with those estimated from
107 the size-dependent aerosol chemical compositions determined by an Aerodyne high-resolution
108 Time-of-Flight Aerosol Mass Spectrometer (HR-ToF-AMS, hereafter as AMS). Assuming
109 internal mixtures, we carried out closure studies on N_{CCN} prediction based on the size-
110 distributions of N_{CN} measured by a TSI SMPS and on the hygroscopicity values derived from
111 size resolved and size integrated chemical compositions measured by AMS using Köhler theory,

112 κ_{AMS} , and some assumed constants. Finally, using the average D_{50} and the size-resolved CCN
113 activation ratios from the CCN measurements, we examined the relative importance of
114 hygroscopicity and mixing state in N_{CCN} predictions at different SS . Hygroscopicity is
115 technically a property of aerosols and it is determined by their chemical composition, mixing
116 state, and size distribution. In this paper, we refer hygroscopicity as a property of the
117 components, assuming internal mixing, in aerosols for the discussions below.

118

119 **2 Experimental methods**

120 **2.1 Sampling site and meteorological conditions**

121 Measurements of aerosol chemical properties and CCN activity were carried out throughout
122 the entire month of May 2011 at the Air Quality Research Supersite situated on the campus of
123 the Hong Kong University of Science and Technology (HKUST) on the east coast of Hong
124 Kong (see <http://www.envr.ust.hk/research/research-facility/background-materials.html>). High
125 relative humidity (RH) with a mean of 81% and an average temperature of 26.0 °C prevailed in
126 this study. More information on the sampling location and meteorological conditions is
127 available from Lee et al. (2013) and Li et al. (2013). Hygroscopic TDMA measurements have
128 also been reported at this site (Lopez-Yglesias et al., 2014; Yeung et al., 2014).

129

130 **2.2 Instrument setup**

131 **2.2.1 Sample Inlet System**

132 Ambient air was sampled at a flow rate of 16.67 L/min after passing through a PM2.5
133 cyclone on the roof of the Supersite (appropriately 20 m above sea level) and into a stainless
134 steel sampling port supplying the on-line instruments of the TSI SMPS, the Droplet
135 Measurement Technologies (DMT) dual column continuous-flow CCN counter (CCNc-200)
136 and the Aerodyne AMS. The sampled air passed through a 1-m long diffusion drier (BMI, San
137 Francisco, CA) filled with silica gel, thus its RH was below 30% before it went into the above
138 instruments for measurements.

139

140 2.2.2 CCN measurements

141 Size-resolved CCN spectra and activation ratios were measured with the CCNc-200 (Lance
142 et al., 2006; Roberts and Nenes, 2005) coupled with a TSI SMPS, consisting of a differential
143 mobility analyzer (DMA, TSI 3081L) and a water-based condensation particle counter (WCPC,
144 TSI 3785).

145 As shown in Fig.1, charge-neutralized aerosols passed through the DMA for classification.
146 The classified aerosols were then split into two streams: with one going into the WCPC for N_{CN}
147 measurements and the other into the CCNc-200 for N_{CCN} measurements. The particle size
148 distribution was measured every 6 min, with an up-scan time of 300 s. The sample flow rate
149 was 1 L/min for the DMA, 0.5 L/min for the WCPC and the CCNc-200 each, and the closed-
150 loop sheath air flow rate was 10 L/min. These flow rate settings allow SMPS (DMA+WCPC)
151 measurements for particles ranging from 7 nm to 300 nm in mobility diameter (D_m), which as
152 we will show later, cover the D_{50} (D_m) range of the particles studied. The sheath flow rate was
153 continuously corrected using a mass flow controller. All flow rates were regularly checked and
154 sizing accuracy for the SMPS and the CCNc-200 was verified with Polystyrene latex (PSL)
155 spheres.

156 The CCNc-200 was operated at a total flow rate of 1 L/min, of which 0.5 L/min was for
157 column A connected to the DMA to measure the size-resolved CCN spectrum and another 0.5
158 L/min was for column B connected to the sample inlet system to measure the total N_{CCN} . A
159 sheath-to-aerosol flow ratio of 10 was used. Lathem and Nenes (2011) pointed out that the
160 direct measurements could lead to underestimations of bulk N_{CCN} due to the depletion of water
161 inside the column by a large amount of aerosols and recommended the use of size-resolved
162 CCN measurement. In our measurements, the bulk N_{CCN} integrated from size-resolved CCN
163 measurement using column A are usually fewer than 5000 cm^{-3} and they correlate well with
164 that from the direct measurement using column B with a slope of 0.97 and correlation
165 coefficient (R^2) of 0.53 as shown in Fig.S1. We use bulk N_{CCN} calculated from column A for the

166 comparison with N_{CN} from SMPS and for the closure study below. For every measurement
167 cycle, four SS (0.15%, 0.35%, 0.50%, and 0.70%) were selected. Measurements at $SS = 0.15\%$
168 lasted 22 min whereas those at other SS lasted 12 min each for repeatability. CCNc temperature
169 transients during SS changes are known to produce unreliable spectra if they occur during a
170 voltage up-scan (Moore et al., 2010). In our measurements, the instrument profiles were
171 allowed up to ~ 2 min to stabilize whenever the temperature gradient was changed. At $SS =$
172 0.15%, a longer time (~ 4 min) was required for the stabilization of temperatures. Only data
173 collected under stabilized temperatures were used for analysis.

174 The CCNc-200 was calibrated with size selected DMA ammonium sulfate particles at the
175 four SS (Deng et al., 2011; Rose et al., 2008) regularly during the campaign. The instrument SS
176 was derived from Köhler theory using a constant van't Hoff factor of 2.5 for ammonium sulfate
177 (Low, 1969; Tang and Munkelwitz, 1994; Young and Warren, 1992).

178

179 **2.2.3 Aerosol chemical compositions**

180 Non-refractory PM_1 (NR- PM_1) constituents of sulfate, nitrate, ammonium, chloride, and
181 organics were measured with the AMS operated under V, pToF, and W modes. The principle
182 behind the instrument has been described in detail elsewhere (DeCarlo et al., 2006) and will
183 only be briefly described here. In pToF mode, the instrument performs particle sizing based on
184 particle time-of-flight with the aid of a chopper and gives size-resolved chemical composition
185 data in vacuum aerodynamic diameter (D_{va}) (DeCarlo et al., 2004). In V mode, the shorter
186 traveling path for ions in the ion time-of-flight (ToF) chamber gives a mass spectral resolving
187 power of approximately 2000 (DeCarlo et al., 2006) and better sensitivity. In W mode, the mass
188 spectral resolving power is approximately 4000 (DeCarlo et al., 2006) but the signal-to-noise
189 ratio is lower. The instrument was operated alternately between the V+pToF combined mode
190 and the W mode for 5 min each. Evaluation of the ionization efficiency (IE) was carried out
191 with ammonium nitrate particles weekly and both the flow rate and particle sizing were
192 calibrated before and after the campaign. A more detailed description of the performance of the

193 AMS during the campaign is presented by Li et al. (2013) and Lee et al. (2013). The AMS only
194 measures NR-species but not elemental carbon (EC), sea salt, or crustal species. However, EC
195 only accounts for less than 5% of the PM1 mass and hence can be neglected (Huang et al., 2014;
196 Lee et al., 2013). Sea salt and crustal species typically exist in the coarse mode and make
197 negligible contributions to PM1.

198

199 **2.3 Data analysis**

200 **2.3.1 CN and CCN data**

201 The time series of N_{CN} and N_{CCN} distributions were obtained using the TSI Aerosol
202 Instrument Manager (AIM) software (Wang and Flagan, 1989) and CCN acquisition software,
203 respectively. The data collected during the voltage up-scan were employed for the inversion.
204 The Scanning Mobility CCN Analysis (SMCA) was employed for calculating the size-resolved
205 CCN activation fractions (Moore et al., 2010). The ratio of N_{CCN} to N_{CN} gives the size-resolved
206 CCN activation fraction at each size. Then, the size-resolved CCN activation ratio was obtained
207 by fitting the activation fraction with the sigmoidal function described by Equation 1 (see
208 section 2.3.3) (Moore et al., 2010; Padró et al., 2010).

209

210 **2.3.2 HR-ToF-AMS data**

211 The standard toolkit of SQUIRREL (Sueper, 2011) was used for AMS data analysis. The
212 collection efficiency (CE) used for this work was 0.5 and the relative ionization efficiency (RIE)
213 of 1.2 for sulfate, 1.1 for nitrate, 1.3 for chloride, 1.4 for organics and 4.0 for ammonium were
214 used as described by Li et al. (2013) and Lee et al. (2013). The size-resolved mass spectra for
215 vacuum aerodynamic diameter (D_{va}) ranging from 50 nm to 2000 nm (DeCarlo et al., 2004) were
216 obtained every 5 min on average. The mass concentration of each size bin was obtained by
217 averaging with the two adjacent size bins to reduce the influence of noise (Rose et al., 2011). In
218 order to relate the size-resolved AMS data with those of SMPS and CCNc measurements directly,

219 the AMS D_{va} size was divided by a factor of 1.7 to obtain the corresponding mobility equivalent
 220 diameter (D_m) (Cheng et al., 2006; DeCarlo et al., 2004). The volume fractions of size-resolved
 221 and bulk chemical compositions were calculated from the mass concentrations using densities of
 222 organics and inorganics of 1.3 g cm^{-3} and 1.75 g cm^{-3} , respectively (Alfarra et al., 2006; Cross et
 223 al., 2007; Gunthe et al., 2009; King et al., 2007).

224

225 **2.3.3 D_{50} , κ_{CCN} and κ_{AMS}**

226 The critical diameter D_{50} , also known as the activation diameter, is the diameter at which 50%
 227 of the particles are activated at a specific SS . The D_{50} of a simple sigmoidal shaped activation
 228 ratio curve is determined by fitting the size-resolved activation fractions with the equation below:

$$229 \quad \frac{N_{CCN}}{N_{CN}} = \frac{B}{1 + \left(\frac{D_p}{D_{50}}\right)^c} \quad (1)$$

230 where D_p is the dry mobility diameter, B , c , and D_{50} are fitting coefficients that describe the
 231 asymptote/plateau, the slope, and the inflection point of the sigmoid, respectively (Moore et al.,
 232 2010; Padró et al., 2012). The values of B were more than 90% during the whole campaign,
 233 indicating most of the particles were in the internal mixing state (Mei et al., 2013).

234 The measured hygroscopic parameter (κ_{CCN}) is determined from D_{50} by:

$$235 \quad \kappa_{CCN} = \frac{4A^3 \sigma_{s/a}(T)}{27T^3 D_{50}^3 \ln^2 S_c} \quad (2)$$

236 where $A = 8.69251 \times 10^{-6} \text{ Km}^3 \text{ J}^{-1}$, $\sigma_{s/a}(T)$ is the temperature-dependent surface tension of the
 237 solution/air interface, T is temperature and S_c is the critical saturation ratio. Pure water surface
 238 tension is assumed in the calculations of κ_{CCN} in this paper (Petters and Kreidenweis, 2013;
 239 Sullivan et al., 2009).

240 The hygroscopic parameter κ_{AMS} can be obtained from AMS measurements using

$$241 \quad \kappa_{AMS} = \kappa_{org} \times f_{org} + \kappa_{inorg} \times f_{inorg} \quad (3)$$

242 where f_{org} and f_{inorg} are the organics and inorganics volume fraction derived from AMS
243 measurements (Petters and Kreidenweis, 2007). Bulk κ_{AMS} (hereafter κ_{AMS_B}) and size-resolved
244 κ_{AMS} (hereafter $\kappa_{\text{AMS}_{SR}}$) are obtained from the corresponding bulk and size-resolved volume
245 fractions of organics and inorganics, respectively. Also, it was assumed that $\kappa_{\text{inorg}} = 0.6$ for the
246 whole campaign, $\kappa_{\text{org}} = 0.2$ for the hazy period and $\kappa_{\text{org}} = 0.1$ for the foggy and non-episode
247 periods.

248 The time-series hygroscopicities derived from bulk and size-resolved AMS measurements
249 are shown in Fig.S2. κ_{AMS_B} were larger than $\kappa_{\text{AMS}_{SR}}$ in all four SS because bulk AMS
250 compositions biased towards the inorganics as discussed below. Their difference increases as SS
251 increases because the corresponding D_{50} decreases and these smaller particles have a larger
252 difference in organic fraction than the bulk has.

253

254 **3 Results and discussion**

255 **3.1 Overview**

256 Fig.2 shows an overview of the bulk N_{CCN} concentrations and $N_{\text{CCN}}/N_{\text{CN}}$ activation ratio at
257 SS of (a) 0.15%, (b) 0.35%, (c) 0.50%, and (d) 0.70%, as well as (e) the bulk N_{CN} and the NR-
258 PM1 total and component mass concentration and (f) the volume fractions of the AMS
259 chemical components over the entire month of May 2011. Statistics of the measurements are
260 given in Table I. The gaps in the data in Fig.2 are due to instrument downtime. For most of the
261 time, the total N_{CCN} at SS of 0.15%, 0.35%, 0.50% and 0.70% were below 800 cm^{-3} , 3000 cm^{-3} ,
262 5000 cm^{-3} and 5600 cm^{-3} respectively, and N_{CN} was below 10000 cm^{-3} . Both N_{CCN} and N_{CN} in
263 this study are lower than those observed in July 2006 in Guangzhou, a nearby city in Southern
264 China (Rose et al., 2010). Large fluctuations in the bulk $N_{\text{CCN}}/N_{\text{CN}}$ ratios were also observed.
265 The bulk $N_{\text{CCN}}/N_{\text{CN}}$ ratio was as low as 0.03 at SS = 0.15%, but it was as high as 0.92 at SS =
266 0.70%. Even at the same SS, the bulk N_{CCN} , N_{CN} and $N_{\text{CCN}}/N_{\text{CN}}$ ratio varied greatly during the
267 campaign.

268 The bulk mass concentrations of NR-PM1 ranged from $0.8 \mu\text{g m}^{-3}$ to $62.4 \mu\text{g m}^{-3}$ with a
269 mean value of $14.5 \pm 9.7 \mu\text{g m}^{-3}$ as shown in Fig.2e. The average bulk volume fractions of NR-
270 species were $53 \pm 10\%$, $25 \pm 13\%$, $18 \pm 4\%$, $4 \pm 3\%$ for sulfate, organics, ammonia, and nitrate,
271 respectively (Lee et al., 2013). The bulk mass concentrations for all NR-species were in general
272 low during the campaign compared with those reported for the PRD region (Gong et al., 2012;
273 Rose et al., 2011; Takegawa et al., 2009; Xiao et al., 2011).

274 There were two periods of particular interest during this campaign: one was a foggy period
275 (May 15) and the other was a hazy period (May 28-30). The division of the month of May in
276 2011 into foggy, hazy and non-episode periods was based on differences in meteorology, such
277 as RH, temperature and cloud cover, and mass concentration and the O:C ratio. On average, the
278 foggy period had a high RH (91.1%), a low temperature ($23.3 \text{ }^\circ\text{C}$) and a high percentage cloud
279 coverage (89.7%) and a high liquid water content (LWC) in fine particles ($47.5 \mu\text{g m}^{-3}$) as
280 shown in Li et al. (2013). The hazy period had a much lower RH (66.6%), a higher temperature
281 ($26.2 \text{ }^\circ\text{C}$) and a much lower percentage cloud coverage (43.3%) and LWC ($17.5 \mu\text{g m}^{-3}$). The
282 slowing surface winds and the establishment of a well-defined land-sea breeze with a gradual
283 daily reversal of wind direction contributed to the accumulation of local and regional pollutants
284 coming from the PRD due to the persistent northerly and northwesterly air masses (Lee et al.,
285 2013).

286 During the foggy period, the bulk NR-PM1 was as high as $30 \mu\text{g m}^{-3}$ (Fig. 2e; Li et al.,
287 2013). The hazy period was much less humid and it saw the highest mass concentration of NR-
288 PM1 species recorded during the whole campaign. The highest degree of oxygenation with
289 average O:C ratio of 0.51 was also obtained (Li et al., 2013). During the hazy period, the mean
290 bulk N_{CCN} ranged from 1100 cm^{-3} with bulk $N_{\text{CCN}}/N_{\text{CN}}$ of 0.22 at $\text{SS} = 0.15\%$ to 5300 cm^{-3} with
291 bulk $N_{\text{CCN}}/N_{\text{CN}}$ of 0.72 at $\text{SS} = 0.70\%$. During non-episode periods, the mean bulk N_{CCN} ranged
292 from 300 cm^{-3} with bulk $N_{\text{CCN}}/N_{\text{CN}}$ of 0.14 at $\text{SS} = 0.15\%$ to 2700 cm^{-3} with bulk $N_{\text{CCN}}/N_{\text{CN}}$ of
293 0.61 at $\text{SS} = 0.70\%$.

294

295 **3.2f, κ_{CCN} and κ_{AMS}**

296 The average size-resolved mass distributions and volume fractions (f) of NR-PM1 calculated
297 from AMS measurements are shown in Fig.3a-c and Fig.3d-f, respectively, for the foggy period,
298 the hazy period, and the non-episode periods. The NR-PM1 showed a major mode at the dry
299 particle size (D_m , hereafter, diameters shown are D_m) of ~285 nm in the foggy period, at ~355
300 nm in the hazy period and at ~325 nm in the non-episode periods. Sulfate and organics
301 accounted for large mass fractions (78% in total) during the whole campaign as shown in Table
302 II. Sulfate dominated in the foggy period, contributing to a volume fraction of 0.45 for 42-200
303 nm particles. Organics and nitrate often had a shoulder at a small size mode at 100 nm to 130 nm.
304 This shoulder was obvious in the hazy period and non-episode periods but not so in the foggy
305 period. On average, this smaller mode accounted for 11% and 12% of organics and nitrate,
306 respectively. On the other hand, only 2% of sulfate was found in this mode (Lee et al., 2013).

307 Fig.3d-f show the average size-resolved volume fraction distributions of the AMS aerosol
308 compositions from 42 nm to 200 nm in the foggy period, the hazy period and the non-episode
309 periods. The volume fraction of organics decreased while the inorganics increased with particle
310 size. Overall, the size-resolved volume fractions of organics ranged from 0.73 at 42 nm to 0.25 at
311 200 nm. Additionally, the bulk volume ratio of organics to inorganics between 42 nm and 200
312 nm was 0.65 in the foggy period, 1.33 in the hazy period, and 0.87 in the non-episode periods.

313 The measured κ_{CCN} (yellow symbols) and the calculated κ_{AMS_SR} (blue symbols), in the form of
314 median values and interquartile ranges, are plotted against their corresponding D_{50} in Fig.3d-f.
315 The median and mean values of κ_{CCN} and κ_{AMS_SR} were essentially the same. Overall, the median
316 D_{50} were 116 nm, 68 nm, 55 nm, and 47 nm, with an interquartile range of less than 16%, at SS
317 of 0.15%, 0.35%, 0.50%, and 0.70%, respectively. During the foggy period, which featured high
318 inorganics volume fractions, the median κ_{CCN} were 0.44, 0.37, 0.36 and 0.29 at SS from 0.15% to
319 0.70%. They are higher than the corresponding values in the hazy period (0.38, 0.36, 0.32 and
320 0.28) and the non-episode periods (0.39, 0.37, 0.33 and 0.27). The difference in κ_{CCN} in these
321 periods was most obvious at $SS = 0.15\%$, at which D_{50} was around 110 nm, and the
322 corresponding inorganic volume fraction was 0.6 in foggy period, 0.4 in the hazy period and 0.5

323 in the non-episode period. The high inorganic volume fraction results in high aerosol
324 hygroscopicity.

325 The $\kappa_{\text{AMS_SR}}$ calculated from Equation 3 assuming $\kappa_{\text{org}} = 0.1$ and $\kappa_{\text{inorg}} = 0.6$ agreed well with
326 the measured κ_{CCN} in the foggy period and the non-episode periods as shown in Fig. 3d and f. In
327 the hazy period (Fig.3e), assuming $\kappa_{\text{org}} = 0.2$ and $\kappa_{\text{inorg}} = 0.6$ gave better agreement between
328 $\kappa_{\text{AMS_SR}}$ and κ_{CCN} . The hazy period had a higher O:C ratio of 0.51, compared to 0.43 and 0.39 in
329 foggy and the non-episode periods respectively (Li et al., 2013), leading to a higher
330 hygroscopicity of the organic aerosols (Chang et al., 2010; Lambe et al., 2011; Massoli et al.,
331 2010; Mei et al., 2013; Moore et al., 2012b).

332 We further examine the correlations between the observed κ_{CCN} and the size-resolved organic
333 volume fraction (f_{org}) in Fig.4a for the hazy period and Fig.4b for the rest of the campaign. In
334 order to avoid the negative impact of low signal-to-noise ratios of AMS measurements on the
335 correlation study, only data points with mass concentrations in a size bin of larger than $0.6 \mu\text{g m}^{-3}$
336 were used. Extrapolation of the least square fit line in Fig.4a and Fig.4b to $f_{\text{org}} = 1$ yields $\kappa_{\text{org}} =$
337 0.21 ± 0.02 and 0.09 ± 0.01 for the organic fraction and extrapolation to $f_{\text{org}} = 0$ yields $\kappa_{\text{inorg}} =$
338 0.59 ± 0.03 and 0.59 ± 0.01 for the inorganic fraction, respectively. These values are close to the
339 characteristic values of organic (0.1) and inorganic hygroscopicity (0.6) in the PRD region (Rose
340 et al., 2011), and to the averaged values of $\kappa_{\text{org}} = 0.1$ and $\kappa_{\text{inorg}} = 0.6 - 0.7$ in earlier studies in
341 Beijing and the Gulf of Mexico (Gunthe et al., 2011; Moore et al., 2012b). The average organic
342 hygroscopicity is within the typical range for individual organic species from zero for insoluble
343 organics to 0.3 for soluble organics (Hersey et al., 2011; Lambe et al., 2011; Petters and
344 Kreidenweis, 2007). $\kappa_{\text{AMS_SR}}$ correlates reasonably well with κ_{CCN} , with R^2 of 0.51, as shown in
345 Fig.S3.

346 On the other hand, the mean value of $\kappa_{\text{AMS_B}}$ derived from bulk AMS compositions was 0.45
347 at $SS = 0.15\%$ and 0.46 for the other SS , which are significantly larger than the measured κ_{CCN}
348 ranging from 0.39 to 0.28 for SS of 0.15% to 0.7% as shown in Table IV. Size-resolved AMS
349 measurements are needed to accurately determine the hygroscopicity parameter and predict N_{CCN}

350 (Cubison et al., 2008; Moore et al., 2012a). For closure analysis shown below, we use $\kappa_{\text{org}} = 0.1$
351 and $\kappa_{\text{inorg}} = 0.6$.

352

353 **3.3 CCN closure study**

354 The closure studies on N_{CCN} prediction were carried out based on the measured size-
355 resolved N_{CN} distributions and the AMS measurements. In the first approach, we assumed
356 internal mixing and used κ_{AMS} from (i) bulk and (ii) the size-resolved AMS measurements for
357 each dataset using Equation 3, and (iii) assumed constant κ values. The corresponding
358 individual D_{50} was then calculated from these κ estimates using Equation 2, based on which
359 N_{CCN} was predicted. Furthermore, we also used the average D_{50} over the whole campaign in
360 N_{CCN} prediction. Table III summarizes the assumptions and parameters used in these methods.
361 In these cases N_{CCN} was calculated by integrating the measured size-resolved N_{CN} distributions
362 for particles larger than D_{50} . The aim of using the average D_{50} was to test how well it
363 represented the activation properties of aerosol during the campaign. Finally, we examined the
364 relative importance of chemical composition and mixing state in N_{CCN} predictions at different
365 SS by comparing the N_{CCN} using the average D_{50} with an internal mixing assumption and the
366 size-resolved CCN activation ratios from CCN measurements which reflect the actual mixing
367 state of the aerosols. The last approach involved integrating the product of the measured size-
368 distribution of N_{CN} and the size-resolved CCN activation ratio in each particle size bin.

369

370 **3.3.1 Prediction of N_{CCN} based on κ_{AMS}**

371 **3.3.1.1 κ_{AMS} from bulk AMS measurements**

372 The hygroscopicity $\kappa_{\text{AMS,B}}$ was estimated by assuming that all particles have the same
373 chemical composition as determined by bulk AMS measurements and $\kappa_{\text{org}} = 0.1$ and $\kappa_{\text{inorg}} = 0.6$.
374 The closure results are shown in Fig.5i a-h and Table IV. Overall, the approaches of using
375 individual D_{50} and the average D_{50} grossly over-predicted N_{CCN} by up to 21% and 26%,
376 respectively. As shown in Fig.3a-c, PM1 was dominated by inorganic species with the bulk

377 volume fraction as high as 69% during the whole period. The bulk volume ratio mainly reflects
378 the composition of particles from 200 to 500 nm where inorganic species dominated. On the
379 other hand, D_{50} at the four SS were all less than 200 nm where organic species accounted for
380 more than 39% of bulk volume fraction as shown in Table II and Fig.3. Therefore, deriving κ_{AMS}
381 from bulk AMS measurements leads to a positive bias toward inorganic species, and hence an
382 overestimation of κ_{AMS_B} and N_{CCN} . Wang et al. (2010) found that the overestimation arising
383 from the use of the bulk mass concentrations decreased from 80% to 39% when SS decreased
384 from 0.35% to 0.11%. Our data also shows decreasing overestimation as SS decreases, except
385 for data at $SS = 0.15\%$, where the N_{CCN} was smaller than 1000 cm^{-3} most of the time. The low
386 counts may have introduced larger uncertainty in the measurements as shown in SI.

387

388 3.3.1.2 κ_{AMS} from size-resolved AMS measurements

389 Fig.5ii a-d and e-h show the correlations between the measured N_{CCN} and the N_{CCN}
390 predicted from the individual D_{50} of each data set and the averaged D_{50} derived from κ_{AMS_SR} ,
391 respectively. The slope and R^2 are given in Table IV. In general, the N_{CCN} prediction deviated
392 by 10% or less for both approaches, a substantial improvement compared to those using κ_{AMS_B} ,
393 and the average D_{50} adequately reflects the aerosol activation properties. At $SS = 0.70\%$,
394 individual D_{50} and the average D_{50} gave the close deviations of 10% and 9% respectively
395 between the measured and predicted N_{CCN} . At high SS , where even particles of moderate
396 hygroscopicity are activated (Kim et al., 2011), the N_{CCN} prediction is less sensitive to
397 hygroscopicity than at low SS . The difference of the deviations increased as SS decreased from
398 0.70% to 0.35%. At lower SS , differences in hygroscopicity as reflected from the different D_{50}
399 used in the calculations gave larger differences in N_{CCN} predictions.

400 The overestimation from using the average D_{50} decreased from 9% at SS of 0.70% ($D_{50} =$
401 46 nm) to 5% and 1% at SS of 0.50% ($D_{50} = 56$ nm) and 0.35% ($D_{50} = 67$ nm), respectively. The
402 fraction of non/less-hygroscopic hydrocarbon-like organic aerosols (HOA) decreased with
403 increasing particle size (Lee et al., 2013). They contribute little to N_{CCN} by themselves but the
404 assumption of internal mixing allows them to contribute to CCN due to their mixing with more

405 hygroscopic species and leads to an overestimated N_{CCN} (Rose et al., 2011; Wang et al., 2010).
406 Size-resolved EC was not available and EC might also have caused the overestimation in N_{CCN}
407 prediction. When SS decreased, D_{50} increased and the impact of HOA on the N_{CCN} predictions
408 decreased because of their smaller abundance relative to the hygroscopic inorganics. The large
409 deviation in N_{CCN} prediction at $SS = 0.15\%$ may be due to the uncertainty in the low number
410 counts of CCN measurements or the high sensitivity of N_{CCN} to hygroscopicity at low SS as
411 discussed later.

412

413 **3.3.2 Prediction of N_{CCN} from the constant κ**

414 A constant $\kappa = 0.30$ has been proposed for predicting N_{CCN} and understanding the indirect
415 effects of continental aerosols on climate on a global modeling scale (Andreae and Rosenfeld,
416 2008; Pringle et al., 2010). Rose et al. (2011) showed that the deviations between the measured
417 and predicted N_{CCN} were less than 20% when they used an averaged $\kappa = 0.30$ over the course of
418 their campaign in PRD in 2006. We evaluated the use of constant $\kappa = 0.30$, 0.33 (the average
419 κ_{AMS_SR} over the campaign at the four SS), and 0.35 to estimate N_{CCN} . Overall, using $\kappa = 0.35$
420 overestimated N_{CCN} at all four SS while using 0.33 and 0.30 underestimated it at low $SS \leq 0.35\%$
421 and overestimated it at high $SS \geq 0.50\%$, respectively, as shown in Fig.S4 and Table IV. The
422 slopes for $\kappa = 0.30$, 0.33 and 0.35 are quite different (0.91, 0.98 and 1.05) at $SS = 0.15\%$, while
423 they are much closer (1.11, 1.12 and 1.13) at $SS = 0.70\%$. The difference in N_{CCN} prediction for
424 the three κ decreased gradually from 14% at $SS = 0.15\%$ to 2% at $SS = 0.70\%$. These results
425 further confirm that the prediction of N_{CCN} is less sensitive to κ at high SS than at low one, and
426 that the impact of hygroscopicity on the N_{CCN} prediction decreases with increasing SS .

427 The difference in the sensitivity of predicted N_{CCN} to hygroscopicity at different SS can also
428 be attributed to the aerosol size distributions (Dusek et al., 2006; Ervens et al., 2007). The
429 average aerosol size distribution over the whole period had a main mode at ~ 70 nm and a
430 shoulder at ~ 30 nm (Fig.6a) in this campaign. At $SS = 0.15\%$, D_{50} is approximately 116 nm and
431 on the right of the main mode (Fig.6b), a slight variation of κ and D_{50} will cause a large change
432 in N_{CCN} prediction. On the contrary, at $SS = 0.70\%$, the corresponding $D_{50} = 46$ nm is on the left

433 of the main mode (Fig.6c), a variation of κ and D_{50} will have less impact on N_{CCN} prediction as
434 the N_{CCN} is dominated by the mode at 70 nm.

435 In addition, we carried out the N_{CCN} prediction during the hazy period, when HOA
436 contributes to ~25% of OA (Li et al, 2013), based on the average size-resolved (1) $\kappa_{AMS} = 0.33$
437 over the whole campaign period and (2) $\kappa_{AMS} = 0.35$ over the hazy period only. As shown in Fig.
438 S5, using $\kappa_{AMS} = 0.33$ and 0.35 gave similar results with overestimations of 14% and 13% at $SS =$
439 0.70% respectively. In the hazy period, the assumption of internal mixing state allowed HOA
440 containing particles to act as CCN, thereby resulting in an overestimation of N_{CCN} by up to 14%.
441 At $SS = 0.15\%$, using $\kappa = 0.33$ led to an overestimation of just 2%, while an overestimation of
442 9% was found when using $\kappa = 0.35$. Overall, using $\kappa = 0.33$ gave predictions of N_{CCN} (Table IV)
443 comparable to those using the κ_{AMS_SR} and better than those using κ_{AMS_B} at all four SS .

444

445 3.3.3 Mixing state and hygroscopicity

446 As discussed earlier, closure analysis based on hygroscopicity or D_{50} derived from chemical
447 compositions alone cannot account for variability in the mixing state of aerosols, which could
448 cause significant differences between predicted and measured N_{CCN} . In this section, we first
449 calculate N_{CCN} by integrating the measured size-resolved N_{CN} distributions above the average
450 D_{50} , obtained from the average CCN size-resolved activation ratio over the whole campaign.
451 The second method involves integrating the product of the measured size-distribution of N_{CN}
452 and the average size-resolved N_{CCN}/N_{CN} activation ratio in each particle size bin. The size-
453 resolved N_{CCN}/N_{CN} activation ratios reflect the influences of both the size-resolved chemical
454 compositions and mixing state on CCN activity, and thus can potentially exclude the impact of
455 non/less hygroscopic species on N_{CCN} prediction and be used to examine the relative importance
456 of mixing state and hygroscopicity in closure analysis compared to predictions assuming
457 internal mixing state (Deng et al., 2013). The first method involves the hygroscopicity of
458 aerosols as reflected by the value of D_{50} and the assumption of internal mixing while the second
459 method involves hygroscopicity with actual mixing state information imbedded in the measured
460 activation ratio curves. A comparison of the predictions of these two methods would give hints

461 to the role of assumption of mixing states. Since D_{50} was obtained from the sigmoidal fits, those
462 fits instead of actual data points were also used in the second method for better comparison.
463 The average size-resolved CCN activation ratios at the four SS over the whole campaign are
464 shown in Fig.S6. Data points are shown as means \pm standard deviations.

465 The correlations of measured and predicted N_{CCN} based on the average D_{50} (a-d) and the
466 average size-resolved activation ratio (e-h) are shown in Fig.5 iii a-d and e-h. The slopes of the
467 fitted lines and R^2 at different SS are given in Table IV. The predicted and the measured N_{CCN}
468 differed by less than 10% using the average D_{50} . The difference is comparable to those using the
469 average D_{50} from κ_{AMS_SR} (Fig.5ii e-h). At $SS = 0.70\%$, using the average size-resolved CCN
470 activation ratios reduced the overestimation from 8% when using the average D_{50} to 4%. As
471 discussed above, the sensitivity of the N_{CCN} prediction to hygroscopicity is low at $SS = 0.70\%$,
472 where a large change of 25% in hygroscopicity from 0.28 to 0.35 result in only a variation within
473 5% in N_{CCN} (Table IV). From the AMS measurements, the portion of non/less-hygroscopic
474 species inferred by the fractions of f_{43} and f_{57} increased as the particle size decreased (Lee et al.,
475 2013). Because of their higher abundance, their mixing with the hygroscopic components has a
476 higher impact at $SS = 0.70\%$ ($D_{50} = 46$ nm) than that at low $SS = 0.15\%$ ($D_{50} = 116$ nm), where
477 the reduction in the overestimation is minimal, from 10% when using the average D_{50} to 9%
478 when using the average activation ratios approach. On the contrary, a difference of 19% was
479 found when hygroscopicity increased from 0.30 to 0.39 at this low SS .

480 The average size-resolved activation ratios during the hazy, foggy and non-episode periods
481 at $SS=0.15\%$ and 0.7% are shown in Fig. 7. At $SS=0.15\%$, the activation ratios during the hazy
482 and non-episode periods are similar but it is higher during the foggy period due possibly to the
483 higher volume fraction of inorganics (Fig. 3d-f) and the smaller amount of non/less hygroscopic
484 organics (Li et al., 2013). At $SS=0.70\%$, the CCN activation ratios of particles ranging from 50
485 nm to 100 nm in size are lower in the hazy period than in the non-episode period. The difference
486 in the trends at $SS=0.15\%$ and 0.70% may be due to the larger fractions of non/less hygroscopic
487 species in smaller particles in the hazy period. These particles, which constitute a larger fraction
488 of OA in the hazy period than in the other periods, likely formed external mixtures containing

489 the aged particles of sulfate and the more oxidized (and hygroscopic) organics. Hence, a larger
490 difference in the activation ratios between the hazy and the other periods could be observed at
491 $SS=0.70\%$ than at $SS=0.15\%$.

492 Fig. 8 shows the N_{CCN} predicted based on the average D_{50} and the average size-resolved CCN
493 activation ratio over the hazy period. At $SS = 0.15\%$, using the average CCN activation ratio
494 reduces overestimation from 12% when using average D_{50} to 10%. However, a much larger
495 reduction from 8% to 1% was found at $SS = 0.70\%$. This comparison supports that N_{CCN}
496 prediction is likely more sensitive to mixing state than to hygroscopicity at high SS and vice
497 versa at low SS .

498

499 **4 Conclusion**

500 In this study, a DMT CCNc-200 for N_{CCN} measurement, a TSI SMPS for N_{CN} measurement,
501 and an Aerodyne HR-ToF-AMS for size-resolved and bulk PM1 chemical composition
502 measurement were used to investigate the size-resolved CCN activity at a coastal site in Hong
503 Kong in May 2011. Closure studies were carried out based on the κ_{AMS} estimated from bulk and
504 size-resolved AMS measurement assuming internal mixing state. The deviation of N_{CCN}
505 predicted from the individual D_{50} obtained from κ_{AMS} was similar to that predicted from the
506 average D_{50} over the whole period at the four SS , which indicates that the average D_{50} well
507 represented the aerosol CCN activation properties in this study. Using $\kappa_{AMS,B}$ grossly over-
508 predicted N_{CCN} by up to 26% because of the positive bias toward the inorganic fraction. On the
509 contrary, the N_{CCN} prediction based on $\kappa_{AMS,SR}$ was within 10% of the measurements. An
510 accurate description of κ incorporating size-dependent compositions is necessary for good N_{CCN}
511 predictions.

512 We compared the sensitivity of the N_{CCN} prediction to hygroscopicity (based on assumed
513 internal mixing and κ estimates) and mixing state at different SS . N_{CCN} appears to be more
514 sensitive to hygroscopicity than to mixing state at $SS = 0.15\%$ but the reverse is true at $SS =$
515 0.70% . At $SS = 0.15\%$, D_{50} (116nm) is larger than the mode diameter of the typical aerosol

516 distributions we observed. A slight variation in κ (and D_{50}) would have a larger effect on N_{CCN}
517 prediction than would at high $SS = 0.70\%$, where D_{50} (46 nm) is smaller than the mode diameter.
518 The effect of mixing state is larger at $SS = 0.70\%$, which is associated with smaller particles
519 having a higher percentage of non/less-hygroscopic components, than at $SS = 0.15\%$.
520 hygroscopicity is relatively less important to N_{CCN} prediction at this high SS .

521

522 **5 Acknowledgments**

523 This work was supported by the University Grants Committee (Special Equipment Grant,
524 SEG-HKUST07), Research Grants Council (GRF 600413) and the Environmental Conservation
525 Funds (ECF) of Hong Kong (project number: ECWW09EG04).

526

527

528

529

530

531

532

533

534

535

536

537

538 **References**

- 539 Alfara, M. R., Paulsen, D., Gysel, M., Garforth, A. A., Dommen, J., Prévôt, A. S., Worsnop, D. R.,
540 Baltensperger, U., and Coe, H.: A mass spectrometric study of secondary organic aerosols
541 formed from the photooxidation of anthropogenic and biogenic precursors in a reaction chamber,
542 *Atmos. Chem. Phys.*, 6, 5279-5293, doi:10.5194/acp-6-5279-2006, 2006.
- 543 Andreae, M., O and Rosenfeld, D.: Aerosol–cloud–precipitation interactions. Part 1. The nature and
544 sources of cloud-active aerosols, *Earth-Sci. Rev.*, 89, 13-41, 2008.
- 545 Asa-Awuku, A., Nenes, A., Gao, S., Flagan, R. C., and Seinfeld, J. H.: Water-soluble SOA from
546 Alkene ozonolysis: composition and droplet activation kinetics inferences from analysis of CCN
547 activity, *Atmos. Chem. Phys.*, 10, 1585-1597, doi:10.5194/acp-10-1585-2010, 2010.
- 548 Asa-Awuku, A., Moore, R. H., Nenes, A., Bahreini, R., Holloway, J. S., Brock, C. A., Middlebrook,
549 A. M., Ryerson, T. B., Jimenez, J. L., and DeCarlo, P. F.: Airborne cloud condensation nuclei
550 measurements during the 2006 Texas Air Quality Study, *J. Geophys. Res-Atmos.*, 116, D11201,
551 doi:10.1029/2010jd014874, 2011.
- 552 Bougiatioti, A., Fountoukis, C., Kalivitis, N., Pandis, S., Nenes, A., and Mihalopoulos, N.: Cloud
553 condensation nuclei measurements in the marine boundary layer of the Eastern Mediterranean:
554 CCN closure and droplet growth kinetics, *Atmos. Chem. Phys.*, 9, 7053-7066, doi:10.5194/acp-
555 9-7053-2009, 2009.
- 556 Chan, C. K. and Yao, X.: Air pollution in mega cities in China, *Atmos. Environ.*, 42, 1-42, 2008.
- 557 Chang, R. Y-W., Slowik, J. G., Shantz, N. C., Vlasenko, A., Liggio, J., Sjostedt, S. J., Leaitch, W.
558 R., and Abbatt, J. P. D.: The hygroscopicity parameter (κ) of ambient organic aerosol at a field
559 site subject to biogenic and anthropogenic influences: relationship to degree of aerosol oxidation,
560 *Atmos. Chem. Phys.*, 10, 5047-5064, doi:10.5194/acp-10-5047-2010, 2010.
- 561 Cheng, Y. F., Eichler, H., Wiedensohler, A., Heintzenberg, J., Zhang, Y. H., Hu, M., Herrmann, H.,
562 Zeng, L. M., Liu, S., and Gnauk, T.: Mixing state of elemental carbon and non-light-absorbing
563 aerosol components derived from in situ particle optical properties at Xinken in Pearl River Delta
564 of China, *J. Geophys. Res-Atmos.*, 111, D20204, doi: 10.1029/2005jd006929, 2006.
- 565 Cross, E. S., Slowik, J. G., Davidovits, P., Allan, J. D., Worsnop, D. R., Jayne, J. T., Lewis†, D. K.,
566 Canagaratna, M., and Onasch, T. B.: Laboratory and ambient particle density determinations
567 using light scattering in conjunction with aerosol mass spectrometry, *Aerosol Sci. Technol.*, 41,
568 343-359, 2007.
- 569 Cubison, M. J., Ervens, B., Feingold, G., Docherty, K. S., Ulbrich, I. M., Shields, L., Prather, K.,
570 Hering, S., and Jimenez, J. L.: The influence of chemical composition and mixing state of Los
571 Angeles urban aerosol on CCN number and cloud properties, *Atmos. Chem. Phys.*, 8, 5649-5667,
572 doi:10.5194/acp-8-5649-2008, 2008.
- 573 DeCarlo, P. F., Kimmel, J. R., Trimborn, A., Northway, M. J., Jayne, J. T., Aiken, A. C., Gonin, M.,
574 Fuhrer, K., Horvath, T., Docherty, K. S., Worsnop, D. R., and Jimenez, J. L.: Field-deployable,
575 high-resolution, time-of-flight aerosol mass spectrometer, *Anal. Chem.*, 78, 8281-8289, 2006.
- 576 DeCarlo, P. F., Slowik, J. G., Worsnop, D. R., Davidovits, P., and Jimenez, J. L.: Particle
577 morphology and density characterization by combined mobility and aerodynamic diameter
578 measurements. Part 1: Theory, *Aerosol Sci. Technol.*, 38, 1185-1205, 2004.
- 579 Deng, Z. Z., Zhao, C. S., Ma, N., Liu, P. F., Ran, L., Xu, W. Y., Chen, J., Liang, Z., Liang, S.,
580 Huang, M. Y., Ma, X. C., Zhang, Q., Quan, J. N., Yan, P., Henning, S., Mildenberger, K.,
581 Sommerhage, E., Schäfer, M., Stratmann, F., and Wiedensohler, A.: Size-resolved and bulk

582 activation properties of aerosols in the North China Plain, *Atmos. Chem. Phys.*, 11, 3835-3846,
583 doi:10.5194/acp-11-3835-2011, 2011.

584 Deng, Z. Z., Zhao, C. S., Ma, N., Ran, L., Zhou, G. Q., Lu, D. R., and Zhou, X. J.: An examination
585 of parameterizations for the CCN number concentration based on in situ measurements of
586 aerosol activation properties in the North China Plain, *Atmos. Chem. Phys.*, 13, 6227-6237,
587 doi:10.5194/acp-13-6227-2013, 2013.

588 Dusek, U., Frank, G. P., Hildebrandt, L., Curtius, J., Schneider, J., Walter, S., Chand, D., Drewnick,
589 F., Hings, S., Jung, D., Borrmann, S., and Andreae, M. O.: Size matters more than chemistry for
590 cloud-nucleating ability of aerosol particles, *Science*, 312, 1375-1378, 2006.

591 Ervens, B., Cubison, M., Andrews, E., Feingold, G., Ogren, J., Jimenez, J., Quinn, P., Bates, T.,
592 Wang, J., and Zhang, Q.: CCN predictions using simplified assumptions of organic aerosol
593 composition and mixing state: a synthesis from six different locations, *Atmos. Chem. Phys.*, 10,
594 4795-4807, doi:10.5194/acp-10-4795-2010, 2010.

595 Ervens, B., Cubison, M. J., Andrews, E., Feingold, G., Ogren, J. A., Jimenez, J. L., Quinn, P. K.,
596 Bates, T. S., Wang, J., Zhang, Q., Coe, H., Flynn, M., and Allan, J. D.: Prediction of cloud
597 condensation nucleus number concentration using measurements of aerosol size distributions and
598 composition and light scattering enhancement due to humidity, *J. Geophys. Res.*, 112, D10S32,
599 doi:10.1029/2006JD007426, 2007.

600 Gong, Z., Lan, Z., Xue, L., Zeng, L., He, L., and Huang, X.: Characterization of submicron
601 aerosols in the urban outflow of the central Pearl River Delta region of China, *Front. Environ.*
602 *Sci. Eng.*, 6, 725-733, 2012.

603 Gunthe, S. S., King, S. M., Rose, D., Chen, Q., Roldin, P., Farmer, D. K., Jimenez, J. L., Artaxo, P.,
604 Andreae, M. O., Martin, S. T., and Pöschl, U.: Cloud condensation nuclei in pristine tropical
605 rainforest air of Amazonia: size-resolved measurements and modeling of atmospheric aerosol
606 composition and CCN activity, *Atmos. Chem. Phys.*, 9, 7551-7575, 2009.

607 Gunthe, S. S., Rose, D., Su, H., Garland, R. M., Achtert, P., Nowak, A., Wiedensohler, A., Kuwata,
608 M., Takegawa, N., Kondo, Y., Hu, M., Shao, M., Zhu, T., Andreae, M. O., and Pöschl, U.: Cloud
609 condensation nuclei (CCN) from fresh and aged air pollution in the megacity region of Beijing,
610 *Atmos. Chem. Phys.*, 11, 11023-11039, doi:10.5194/acp-11-11023-2011, 2011.

611 Hersey, S. P., Craven, J. S., Schilling, K. A., Metcalf, A. R., Sorooshian, A., Chan, M. N., Flagan,
612 R. C., and Seinfeld, J. H.: The Pasadena Aerosol Characterization Observatory (PACO):
613 chemical and physical analysis of the Western Los Angeles basin aerosol, *Atmos. Chem. Phys.*,
614 11, 7417-7443, doi:10.5194/acp-11-7417-2011, 2011.

615 Huang, X. H., Bian, Q., Ng, W. M., Louie, P. K., and Yu, J. Z.: Characterization of PM 2.5 Major
616 Components and Source Investigation in Suburban Hong Kong: A One Year Monitoring Study,
617 *Aerosol Air Qual. Res.*, 14, 237-250, 2014.

618 Kammermann, L., Gysel, M., Weingartner, E., Herich, H., Cziczo, D. J., Holst, T., Svenningsson,
619 B., Arneth, A., and Baltensperger, U.: Subarctic atmospheric aerosol composition: 3. Measured
620 and modeled properties of cloud condensation nuclei, *J. Geophys. Res.*, 115, D04202,
621 doi:10.1029/2009JD012447, 2010.

622 Kerminen, V.-M., Paramonov, M., Anttila, T., Riipinen, I., Fountoukis, C., Korhonen, H., Asmi, E.,
623 Laakso, L., Lihavainen, H., and Swietlicki, E.: Cloud condensation nuclei production associated
624 with atmospheric nucleation: a synthesis based on existing literature and new results, *Atmos.*
625 *Chem. Phys.*, 12, 12037-12059, doi:10.5194/acp-12-12037-2012, 2012.

626 Kim, J. H., Yum, S. S., Shim, S., Yoon, S.-C., Hudson, J. G., Park, J., and Lee, S.-J.: On aerosol
627 hygroscopicity, cloud condensation nuclei (CCN) spectra and critical supersaturation measured

628 at two remote islands of Korea between 2006 and 2009, *Atmos. Chem. Phys.*, 11, 12627-12645,
629 doi:10.5194/acp-11-12627-2011, 2011.

630 King, S. M., Rosenoern, T., Shilling, J. E., Chen, Q., and Martin, S. T.: Cloud condensation
631 nucleus activity of secondary organic aerosol particles mixed with sulfate, *Geophys. Res. Lett.*,
632 34, L24806, doi:10.1029/2007GL030390, 2007.

633 Lambe, A. T., Onasch, T. B., Massoli, P., Croasdale, D. R., Wright, J. P., Ahern, A. T., Williams, L.
634 R., Worsnop, D. R., Brune, W. H., and Davidovits, P.: Laboratory studies of the chemical
635 composition and cloud condensation nuclei (CCN) activity of secondary organic aerosol (SOA)
636 and oxidized primary organic aerosol (OPOA), *Atmos. Chem. Phys.*, 11, 8913-8928,
637 doi:10.5194/acp-11-8913-2011, 2011.

638 Lance, S., Nenes, A., Mazzoleni, C., Dubey, M. K., Gates, H., Varutbangkul, V., Rissman, T. A.,
639 Murphy, S. M., Sorooshian, A., and Flagan, R. C.: Cloud condensation nuclei activity, closure,
640 and droplet growth kinetics of Houston aerosol during the Gulf of Mexico Atmospheric
641 Composition and Climate Study (GoMACCS), *J. Geophys. Res.*, 114, D00F15,
642 doi:10.1029/2008JD011699, 2009.

643 Lance, S., Nenes, A., Medina, J., and Smith, J. N.: Mapping the operation of the DMT continuous
644 flow CCN counter, *Aerosol Sci. Technol.*, 40, 242-254, 2006.

645 Latham, T. L., Beyersdorf, A. J., Thornhill, K. L., Winstead, E. L., Cubison, M. J., Hecobian, A.,
646 Jimenez, J. L., Weber, R. J., Anderson, B. E., and Nenes, A.: Analysis of CCN activity of Arctic
647 aerosol and Canadian biomass burning during summer 2008, *Atmos. Chem. Phys.*, 13, 2735-
648 2756, doi:10.5194/acp-13-2735-2013, 2013.

649 Latham, T. L. and Nenes, A.: Water vapor depletion in the DMT continuous-flow CCN chamber:
650 Effects on supersaturation and droplet growth, *Aerosol Sci. Technol.*, 45, 604-615, 2011.

651 Lee, B. P., Li, Y. J., Yu, J. Z., Louie, P. K., and Chan, C. K.: Physical and chemical
652 characterization of ambient aerosol by HR-ToF-AMS at a suburban site in Hong Kong during
653 springtime 2011, *J. Geophys. Res.-Atmos.*, 118, 8625-8639, doi:10.1002/jgrd.50658, 2013.

654 Li, Y. J., Lee, B. Y. L., Yu, J. Z., Ng, N. L., and Chan, C. K.: Evaluating the degree of oxygenation
655 of organic aerosol during foggy and hazy days in Hong Kong using high-resolution time-of-
656 flight aerosol mass spectrometry (HR-ToF-AMS), *Atmos. Chem. Phys.*, 13, 8739-8753,
657 doi:10.5194/acp-13-8739-2013, 2013.

658 Li, Y. J., Lee, B. P., Su, L., Fung, J. C. H., and Chan, C. K.: Seasonal characteristics of fine
659 particulate matter (PM) based on high resolution time-of-flight aerosol mass spectrometric (HR-
660 ToF-AMS) measurements at the HKUST Supersite in Hong Kong, *Atmos. Chem. Phys. Discuss.*,
661 14, 20259-20293, doi:10.5194/acpd-14-20259-2014, 2014.

662 Lopez-Yglesias, X. F., Yeung, M. C., Dey, S. E., Brechtel, F. J., and Chan, C. K.: Performance
663 evaluation of the Brechtel Mfg. Humidified Tandem Differential Mobility Analyzer (BMI
664 HTDMA) for studying hygroscopic properties of aerosol particles, *Aerosol Sci. Technol.*, 2014,
665 *accepted*.

666 Low, R. D. H.: A generalized equation for the solution effect in droplet growth, *J. Atmos. Sci.*, 26,
667 608-611, 1969.

668 Massoli, P., Lambe, A. T., Ahern, A. T., Williams, L. R., Ehn, M., Mikkila, J., Canagaratna, M. R.,
669 Brune, W. H., Onasch, T. B., Jayne, J. T., Petaja, T., Kulmala, M., Laaksonen, A., Kolb, C. E.,
670 Davidovits, P., and Worsnop, D. R.: Relationship between aerosol oxidation level and
671 hygroscopic properties of laboratory generated secondary organic aerosol (SOA) particles,
672 *Geophys. Res. Lett.*, 37, L24801, doi:10.1029/2010gl045258, 2010.

673 Medina, J., Nenes, A., Sotiropoulou, R. E. P., Cottrell, L. D., Ziemba, L. D., Beckman, P. J., and
674 Griffin, R. J.: Cloud condensation nuclei closure during the International Consortium for
675 Atmospheric Research on Transport and Transformation 2004 campaign: Effects of size-resolved
676 composition, *J. Geophys. Res.*, 112, D10s31, doi:10.1029/2006jd007588, 2007.

677 Mei, F., Setyan, A., Zhang, Q., and Wang, J.: CCN activity of organic aerosols observed downwind
678 of urban emissions during CARES, *Atmos. Chem. Phys.*, 13, 12155-12169, doi:10.5194/acp-13-
679 12155-2013, 2013.

680 Moore, R. H., Cerully, K., Bahreini, R., Brock, C. A., Middlebrook, A. M., and Nenes, A.:
681 Hygroscopicity and composition of California CCN during summer 2010, *J. Geophys. Res.-*
682 *Atmos.*, 117, D00v12, doi:10.1029/2011jd017352, 2012a.

683 Moore, R. H., Nenes, A., and Medina, J.: Scanning mobility CCN analysis-A method for fast
684 measurements of size-resolved CCN distributions and activation kinetics, *Aerosol Sci. Technol.*,
685 44, 861-871, 2010.

686 Moore, R. H., Raatikainen, T., Langridge, J. M., Bahreini, R., Brock, C. A., Holloway, J. S., Lack,
687 D. A., Middlebrook, A. M., Perring, A. E., Schwarz, J. P., Spackman, J. R., and Nenes, A.: CCN
688 spectra, hygroscopicity, and droplet activation kinetics of secondary organic aerosol resulting
689 from the 2010 Deepwater Horizon oil spill, *Environ. Sci. Technol.*, 46, 3093-3100, 2012b.

690 Padró L. T., Moore, R. H., Zhang, X., Rastogi, N., Weber, R. J., and Nenes, A.: Mixing state and
691 compositional effects on CCN activity and droplet growth kinetics of size-resolved CCN in an
692 urban environment, *Atmos. Chem. Phys.*, 12, 10239-10255, doi:10.5194/acp-12-10239-2012,
693 2012.

694 Padró L. T., Tkacik, D., Lathem, T., Hennigan, C. J., Sullivan, A. P., Weber, R. J., Huey, L. G.,
695 and Nenes, A.: Investigation of cloud condensation nuclei properties and droplet growth kinetics
696 of the water - soluble aerosol fraction in Mexico City, *J. Geophys. Res.-Atmos.*, 115, D09204,
697 doi:10.1029/2009jd013195, 2010.

698 Petters, M. D. and Kreidenweis, S. M.: A single parameter representation of hygroscopic growth
699 and cloud condensation nucleus activity, *Atmos. Chem. Phys.*, 7, 1961-1971, doi:10.5194/acp-8-
700 6273/2008, 2007.

701 Petters, M. D. and Kreidenweis, S. M.: A single parameter representation of hygroscopic growth
702 and cloud condensation nucleus activity-Part 3: Including surfactant partitioning, *Atmos. Chem.*
703 *Phys.*, 13, 1081-1091, doi:10.5194/acp-13-1081-2013, 2013.

704 Pringle, K. J., Tost, H., Pozzer, A., Pöschl, U., and Lelieveld, J.: Global distribution of the effective
705 aerosol hygroscopicity parameter for CCN activation, *Atmos. Chem. Phys.*, 10, 5241-5255,
706 doi:10.5194/acp-10-5241-2010, 2010.

707 Roberts, G. C. and Nenes, A.: A continuous-flow streamwise thermal-gradient CCN chamber for
708 atmospheric measurements, *Aerosol Sci. Technol.*, 39, 206-221, 2005.

709 Rose, D., Gunthe, S. S., Mikhailov, E., Frank, G. P., Dusek, U., Andreae, M. O., and Pöschl, U.:
710 Calibration and measurement uncertainties of a continuous-flow cloud condensation nuclei
711 counter (DMT-CCNC): CCN activation of ammonium sulfate and sodium chloride aerosol
712 particles in theory and experiment, *Atmos. Chem. Phys.*, 8, 1153-1179, doi:10.5194/acp-8-1153-
713 2008, 2008.

714 Rose, D., Gunthe, S. S., Su, H., Garland, R. M., Yang, H., Berghof, M., Cheng, Y. F., Wehner, B.,
715 Achtert, P., Nowak, A., Wiedensohler, A., Takegawa, N., Kondo, Y., Hu, M., Zhang, Y.,
716 Andreae, M. O., and Pöschl, U.: Cloud condensation nuclei in polluted air and biomass burning
717 smoke near the mega-city Guangzhou, China-Part 2: Size-resolved aerosol chemical

718 composition, diurnal cycles, and externally mixed weakly CCN-active soot particles, Atmos.
719 Chem. Phys., 11, 2817-2836, doi:10.5194/acp-11-2817-2011, 2011.

720 Rose, D., Nowak, A., Achtert, P., Wiedensohler, A., Hu, M., Shao, M., Zhang, Y., Andreae, M. O.,
721 and Pöschl, U.: Cloud condensation nuclei in polluted air and biomass burning smoke near the
722 mega-city Guangzhou, China-Part 1: Size-resolved measurements and implications for the
723 modeling of aerosol particle hygroscopicity and CCN activity, Atmos. Chem. Phys., 10, 3365-
724 3383, doi:10.5194/acp-10-3365-2010, 2010.

725 Stroud, C. A., Nenes, A., Jimenez, J. L., DeCarlo, P. F., Huffman, J. A., Bruintjes, R., Nemitz, E.,
726 Delia, A. E., Toohey, D. W., Guenther, A. B., and Nandi, S.: Cloud activating properties of
727 aerosol observed during CELTIC, J. Atmos. Sci., 64, 441-459, 2007.

728 Sueper, D.: ToF-AMS data analysis software: [http://cires.colorado.edu/jimenez-](http://cires.colorado.edu/jimenez-group/ToFAMSResources/ToFSoftware/index.html)
729 [group/ToFAMSResources/ToFSoftware/index.html](http://cires.colorado.edu/jimenez-group/ToFAMSResources/ToFSoftware/index.html), (last access: 1 June, 2012), 2011.

730 Sullivan, R. C., Moore, M. J. K., Petters, M. D., Kreidenweis, S. M., Roberts, G. C., and Prather, K.
731 A.: Effect of chemical mixing state on the hygroscopicity and cloud nucleation properties of
732 calcium mineral dust particles, Atmos. Chem. Phys., 9, 3303-3316, doi:10.5194/acp-9-3303-
733 2009, 2009.

734 Takegawa, N., Miyakawa, T., Watanabe, M., Kondo, Y., Miyazaki, Y., Han, S., Zhao, Y., Van
735 Pinxteren, D., Brüggemann, E., Gnauk, T., Herrmann, H., Xiao, R., Deng, Z., Hu, M., Zhu, T.,
736 and Zhang, Y.: Performance of an Aerodyne aerosol mass spectrometer (AMS) during intensive
737 campaigns in China in the summer of 2006, Aerosol Sci. Technol., 43, 189-204, 2009.

738 Tang, I. N. and Munkelwitz, H. R.: Water activities, densities, and refractive indices of aqueous
739 sulfates and sodium nitrate droplets of atmospheric importance, J. Geophys. Res.-Atmos, 99,
740 18801-18818, doi:10.1029/94jd01345, 1994.

741 Textor, C., Schulz, M., Guibert, S., Kinne, S., Balkanski, Y., Bauer, S., Berntsen, T., Berglen, T.,
742 Boucher, O., Chin, M., Dentener, F., Diehl, T., Easter, R., Feichter, H., Fillmore, D., Ghan, S.,
743 Ginoux, P., Gong, S., Grini, A., Hendricks, J., Horowitz, L., Huang, P., Isaksen, I., Iversen, I.,
744 Kloster, S., Koch, D., Kirkevåg, A., Kristjansson, J. E., Krol, M., Lauer, A., Lamarque, J. F., Liu,
745 X., Montanaro, V., Myhre, G., Penner, J., Pitari, G., Reddy, S., Seland, Ø., Stier, P., Takemura,
746 T., and Tie, X.: Analysis and quantification of the diversities of aerosol life cycles within
747 AeroCom, Atmos. Chem. Phys., 6, 1777-1813, doi:10.5194/acp-6-1777-2006, 2006.

748 Wang, J., Cubison, M. J., Aiken, A. C., Jimenez, J. L., and Collins, D. R.: The importance of
749 aerosol mixing state and size-resolved composition on CCN concentration and the variation of
750 the importance with atmospheric aging of aerosols, Atmos. Chem. Phys., 10, 7267-7283,
751 doi:10.5194/acp-10-7267-2010, 2010.

752 Wang, S. C. and Flagan, R. C.: Scanning electrical mobility spectrometer, Aerosol Sci. Technol.,
753 13, 230-240, 1990.

754 Wex, H., McFiggans, G., Henning, S., and Stratmann, F.: Influence of the external mixing state of
755 atmospheric aerosol on derived CCN number concentrations, Geophys. Res. Lett., 37, L10805,
756 doi:10.1029/2010gl043337, 2010.

757 Xiao, R., Takegawa, N., Zheng, M., Kondo, Y., Miyazaki, Y., Miyakawa, T., Hu, M., Shao, M.,
758 Zeng, L., Gong, Y., Lu, K., Deng, Z., Zhao, Y., and Zhang, Y. H.: Characterization and source
759 apportionment of submicron aerosol with aerosol mass spectrometer during the PRIDE-PRD
760 2006 campaign, Atmos. Chem. Phys., 11, 6911-6929, doi:10.5194/acp-11-6911-2011, 2011.

761 Yeung, M.C., Lee, B.P., Li, Y. J., Chan, C. K.: Simultaneous HTDMA and HR-ToF-AMS
762 measurements at the HKUST Supersite in Hong Kong in 2011”, J. Geophys. Res.-Atmos., 2014,
763 *in press*.

- 764 Young, K. C. and Warren, A. J.: A reexamination of the derivation of the equilibrium
765 supersaturation curve for soluble particles, *J. Atmos. Sci.*, 49, 1138-1143, 1992.
- 766 Zhang, Z., Engling, G., Lin, C.-Y., Chou, C. C.-K., Lung, S.-C. C., Chang, S.-Y., Fan, S., Chan, C.-
767 Y., and Zhang, Y.-H.: Chemical speciation, transport and contribution of biomass burning smoke
768 to ambient aerosol in Guangzhou, a mega city of China, *Atmos. Environ.*, 44, 3187-3195, 2010.

769

770

771

772 Table I. Statistics of the bulk N_{CCN} (cm^{-3}) at four SS (%) showing the minimum, maximum, mean
 773 number concentration, the N_{CCN}/N_{CN} ratio, and standard deviation (SD). The last column shows
 774 the number of samples (n) in this campaign.

SS (%)	Max		Min		Mean \pm SD		n
	N_{CCN} (cm^{-3})	N_{CCN}/N_{CN}	N_{CCN} (cm^{-3})	N_{CCN}/N_{CN}	N_{CCN} (cm^{-3})	N_{CCN}/N_{CN}	
0.15	2815	0.54	33	0.03	512 ± 452	0.16 ± 0.08	319
0.35	8055	0.78	186	0.08	1546 ± 1137	0.48 ± 0.14	316
0.50	9156	0.82	210	0.12	1815 ± 1285	0.57 ± 0.14	326
0.70	9268	0.92	280	0.16	2082 ± 1484	0.65 ± 0.14	320

775

776

777

778

779

780

781

782

783

784

785

786

787

788

789

790

791

792

793 Table II. The average size-resolved mass concentrations ($\mu\text{g m}^{-3}$, Conc.) and volume fractions (f)
 794 of chemical compositions from size-resolved AMS measurements during the foggy, hazy and the
 795 non-episode periods. Conc. and f were obtained by integrating over the size range (D_m) from 42
 796 nm to 1200 nm for Fig.3a-c and from 42 nm to 200 nm for Fig.3d-f. Data are shown as mean \pm
 797 standard deviations.

Period	Organics		Sulfate		Ammonium		Nitrate		Chloride	
	Conc.	f								
Foggy	1.60 \pm 1.10	0.39 \pm 0.12	4.86 \pm 3.51	0.45 \pm 0.10	1.33 \pm 0.98	0.14 \pm 0.04	0.18 \pm 0.12	0.03 \pm 0.00	0.03 \pm 0.02	0.001 \pm 0.00
Hazy	4.25 \pm 2.52	0.57 \pm 0.08	5.96 \pm 4.36	0.29 \pm 0.06	1.71 \pm 1.22	0.08 \pm 0.03	0.51 \pm 0.27	0.06 \pm 0.01	0.02 \pm 0.01	0.002 \pm 0.00
The rest	1.19 \pm 0.71	0.47 \pm 0.11	2.65 \pm 1.86	0.37 \pm 0.08	0.81 \pm 0.55	0.12 \pm 0.03	0.25 \pm 0.15	0.04 \pm 0.00	0.02 \pm 0.01	0.002 \pm 0.00

798
 799
 800
 801
 802
 803
 804
 805
 806
 807
 808
 809
 810
 811
 812
 813
 814
 815

816 Table III. Methods used in N_{CCN} prediction based on the individual and average D_{50} over whole
 817 period from AMS measurement.

Methods	Mixing state	Chemical composition	κ_{AMS}	D_{50}
I	Internal	Bulk AMS measurements		Individual
II	Internal	Bulk AMS measurements	$\kappa_{AMS} = 0.1 \times f_{org} + 0.6 \times f_{inorg}$	Average
III	Internal	Size-resolved AMS measurements		Individual
IV	Internal	Size-resolved AMS measurements		Average
V	Internal	N/A	0.35/0.33/0.30	Constants

818

819

820

821

822

823

824

825

826

827

828

829

830

831

832

833

834

835 Table IV. Overview of N_{CCN} predictions, κ from D_{50} based on CCN measurement and derived
 836 from equation 3 based on AMS measurement are shown as mean \pm standard deviation, slope
 837 and R^2 are from the least square fit between the calculated N_{CCN} and measured ones.

Categories	Principles	SS (%)	κ	Slope	R^2
CCN _C	The average D_{50} from CCN measurement	0.15	0.39 ± 0.06	1.10	0.94
		0.35	0.36 ± 0.09	1.01	0.95
		0.50	0.31 ± 0.10	1.05	0.97
		0.70	0.28 ± 0.09	1.08	0.98
	The average CCN activation ratio	0.15	-	1.09	0.94
		0.35	-	0.99	0.95
		0.50	-	1.02	0.97
		0.70	-	1.04	0.98
AMS	The D_{50} from κ_{AMS_B}	0.15	-	1.21	0.93
		0.35	-	1.06	0.95
		0.50	-	1.13	0.96
		0.70	-	1.17	0.98
	The average D_{50} from κ_{AMS_B}	0.15	0.45 ± 0.07	1.26	0.93
		0.35	0.46 ± 0.06	1.08	0.96
		0.50	0.46 ± 0.06	1.13	0.96
		0.70	0.46 ± 0.07	1.18	0.98
	The D_{50} from κ_{AMS_SR}	0.15	-	1.06	0.91
		0.35	-	0.94	0.93
		0.50	-	1.03	0.95
		0.70	-	1.10	0.97
The average D_{50} from κ_{AMS_SR}	0.15	0.37 ± 0.07	1.08	0.94	
	0.35	0.35 ± 0.08	1.01	0.95	
	0.50	0.31 ± 0.07	1.05	0.97	
	0.70	0.29 ± 0.09	1.09	0.98	
Others	Constant κ	0.15	0.35/0.33/0.30	1.05/0.98/0.91	0.95/0.95/0.95
		0.35	0.35/0.33/0.30	1.01/0.96/0.91	0.95/0.95/0.95
		0.50	0.35/0.33/0.30	1.08/1.05/1.03	0.97/0.97/0.97
		0.70	0.35/0.33/0.30	1.13/1.12/1.11	0.98/0.98/0.98

838

839 **Figure Captions**

840 Fig.1. Schematic of the experimental setup for size-resolved CCN activation and chemical
841 composition measurement.

842 Fig.2. The N_{CCN} and the $N_{\text{CCN}}/N_{\text{CN}}$ ratio at *SS* of (a) 0.15%, (b) 0.35%, (c) 0.50%, and (d) 0.70%;
843 (e) N_{CN} and NR-species mass concentrations from CCNc, SMPS and AMS; (f) NR-species
844 volume fractions derived from AMS.

845 Fig.3. Size-resolved mass concentration distributions of aerosol chemical composition derived
846 from AMS averaged over (a) the foggy period, (b) the hazy period, and (c) the non-episode
847 periods; the corresponding size-resolved volume fractions of aerosol chemical compositions
848 (colored areas), the observed κ_{CCN} (yellow) and the calculated $\kappa_{\text{AMS_SR}}$ (blue) during (d) the foggy
849 period, (e) the hazy period and (g) the non-episode period. Data points median values and
850 interquartile ranges. $\kappa_{\text{inorg}} = 0.6$ in all cases, $\kappa_{\text{org}} = 0.1$ in (d) and (f), $\kappa_{\text{org}} = 0.2$ in (e).

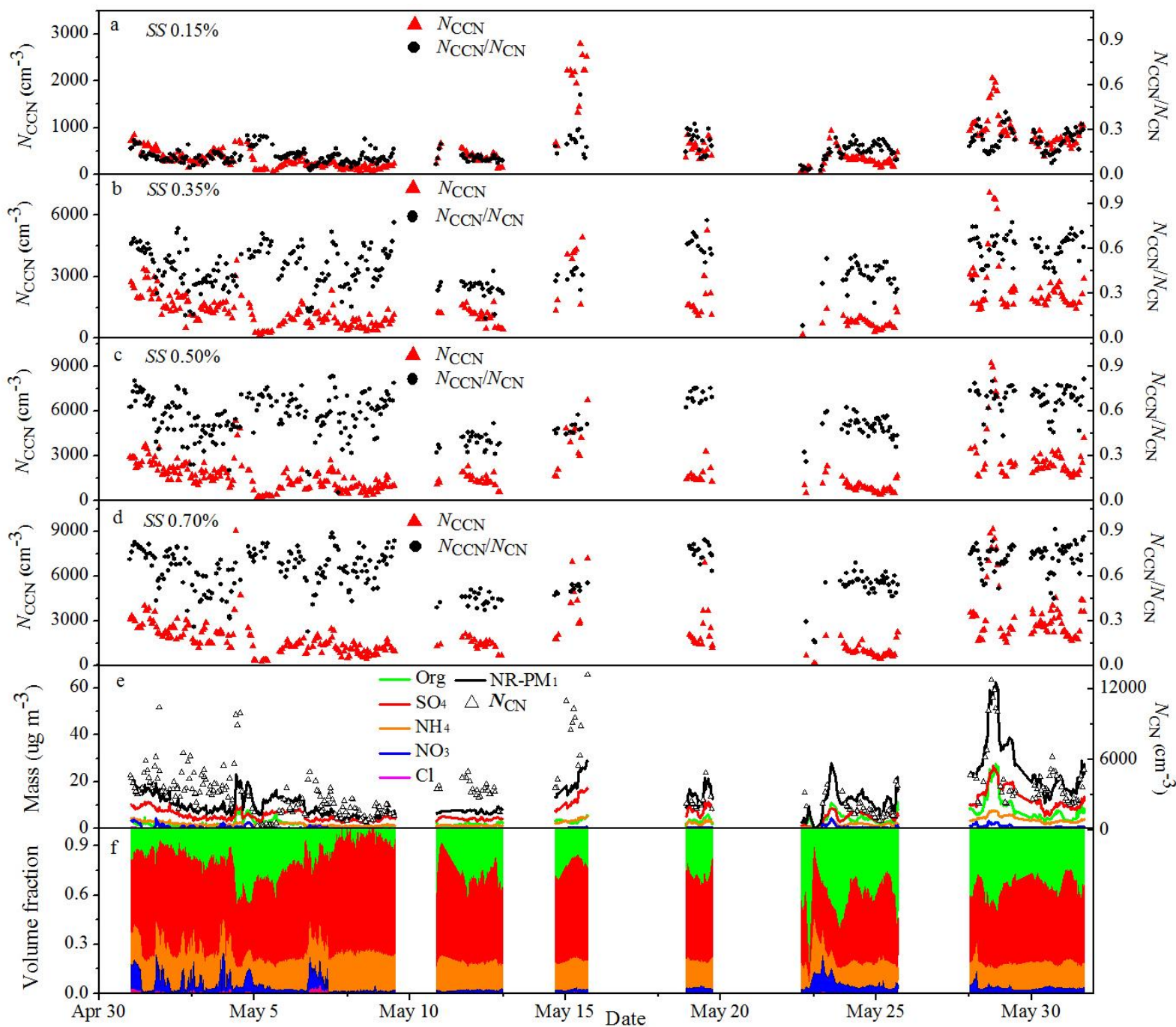
851 Fig.4. Correlations between the observed κ_{CCN} and the organic volume fraction (f_{org}) determined
852 by size-resolved AMS measurements for the (a) hazy period ($n = 72$) and (b) the non-episode
853 period ($n = 516$). The red line is the linear least squares fit (p-value < 0.01) shown in figure.

854 Fig.5. Calculations of N_{CCN} based on i (a-d) the individual D_{50} and (e-h) the average D_{50} over the
855 whole period from $\kappa_{\text{AMS_B}}$, ii (a-d) the individual D_{50} and (e-h) the average D_{50} over the whole
856 period from $\kappa_{\text{AMS_SR}}$ and iii (a-d) the average D_{50} and (e-h) the average size-resolved CCN
857 activation ratio from CCN measurement over the whole period.

858 Fig.6. The average aerosol size distribution over the whole period (a), N_{CCN} prediction based on
859 D_{50} at *SS* of (b) 0.15% and (c) 0.70%. Data points are mean values and standard deviation.

860 Fig.7. The average size-resolved CCN activation ratio at *SS* of (a) 0.15% and (b) 0.70% during
861 the hazy, foggy and non-episode periods.

862 Fig.8. N_{CCN} estimation in hazy period based on (a and b) the average D_{50} and (c and d) the
863 average size-resolved CCN activation ratio from CCN measurement over the hazy period.



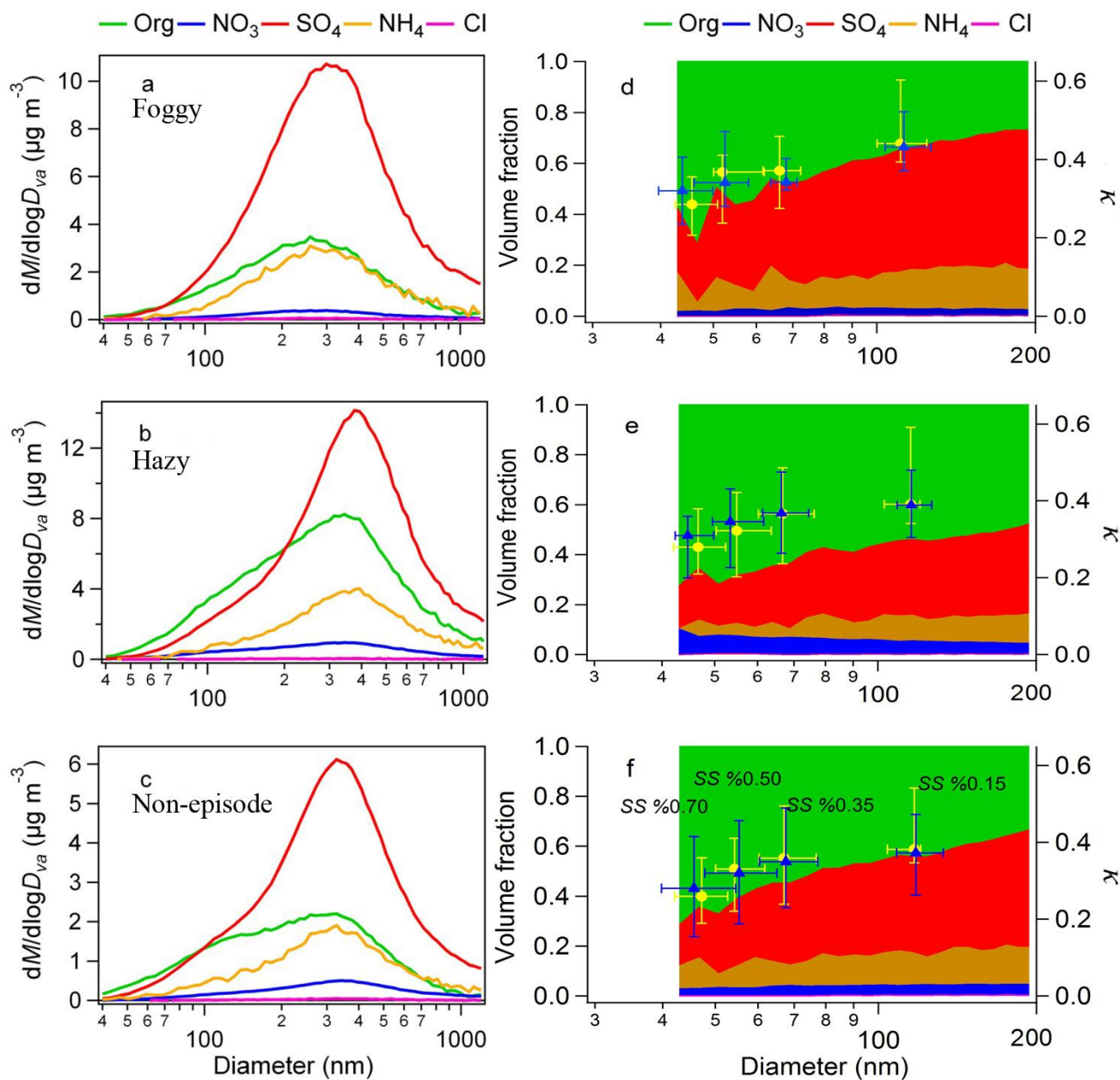
874

875

876 Fig.2. The N_{CCN} and the N_{CCN}/N_{CN} ratio at SS of (a) 0.15%, (b) 0.35%, (c) 0.50%, and (d) 0.70%; (e)

877 N_{CN} and NR-species mass concentration derived from CCNc, SMPS and AMS respectively; (f) NR-

878 species volume fraction derived from AMS.

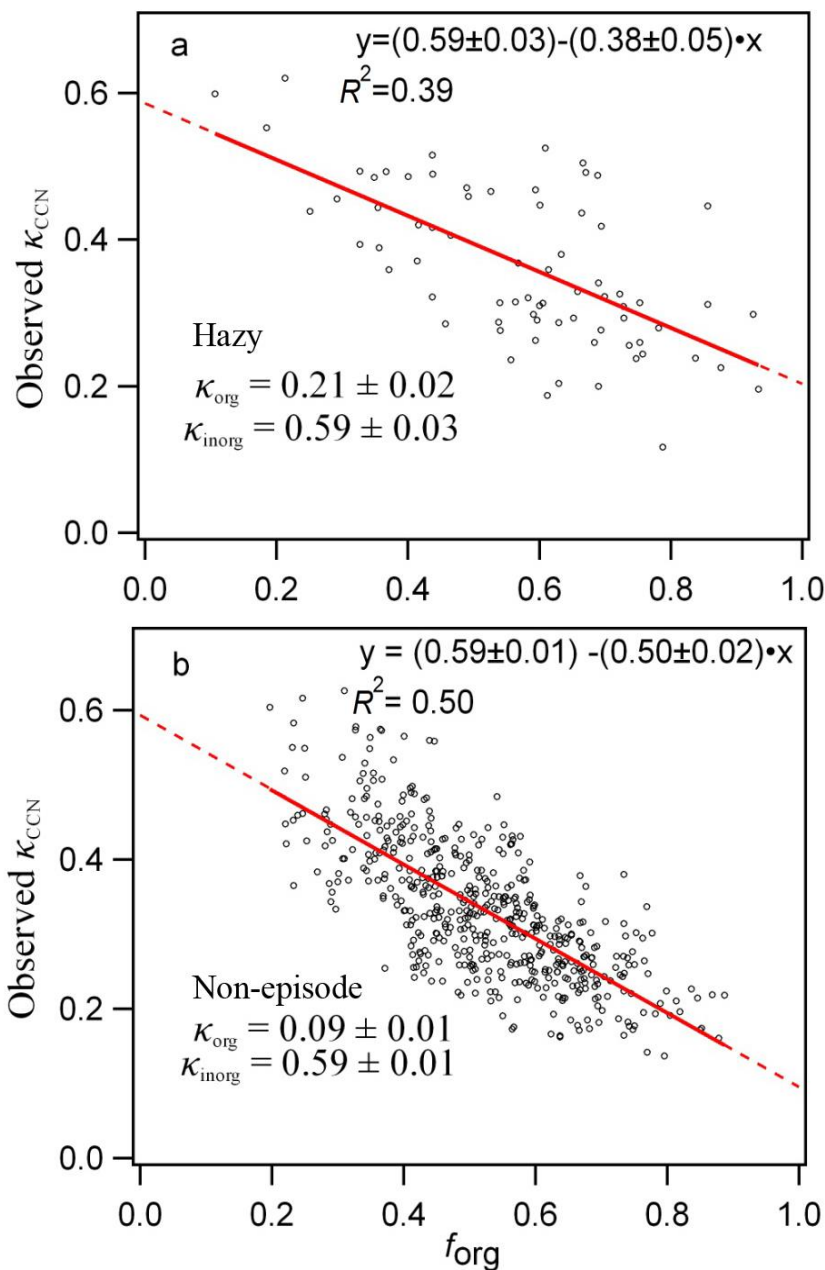


879

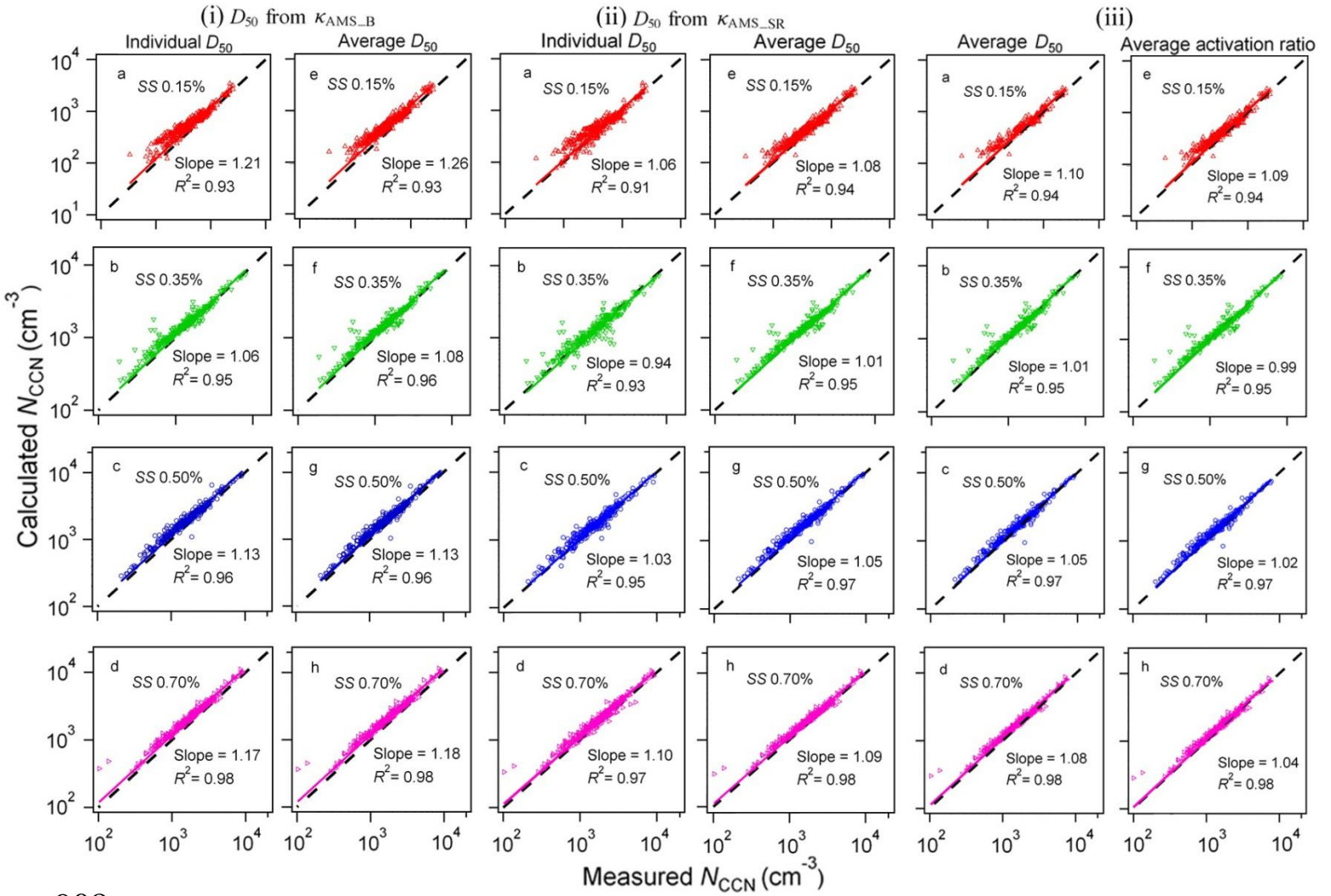
880

881 Fig.3. Size-resolved mass concentration distributions of aerosol chemical composition derived
 882 from AMS averaged over (a) the foggy period, (b) the hazy period, and (c) the non-episode
 883 periods; the corresponding size-resolved volume fractions of aerosol chemical compositions
 884 (colored areas) and the observed κ_{CCN} (yellow) and the calculated κ_{AMS_SR} (blue) during (d) the
 885 foggy period, (e) the hazy period and (f) the non-episode period. Data points are median values
 886 and interquartile ranges. $\kappa_{inorg} = 0.6$ in all cases, $\kappa_{org} = 0.1$ in (d) and (f), and $\kappa_{org} = 0.2$ in (e).

887
888
889
890
891
892
893
894
895
896
897
898
899
900
901
902
903
904



905 Fig.4. Correlations between the observed κ_{CCN} and the organic volume fraction (f_{org}) determined
906 by size-resolved AMS measurements for the (a) hazy period ($n = 72$) and (b) the non-episode
907 period ($n = 516$). The red line is the linear least squares fit (p-value < 0.01) shown in figure.



908

909

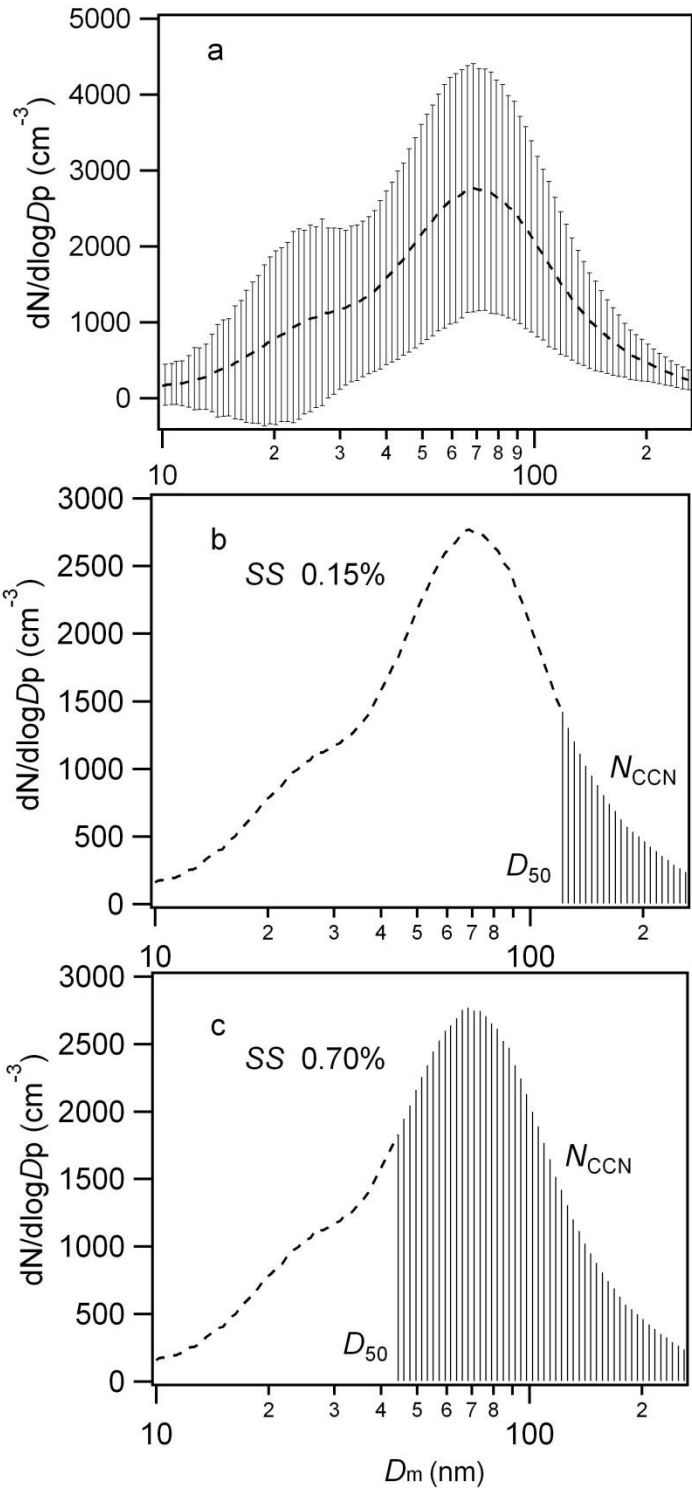
910

911

912

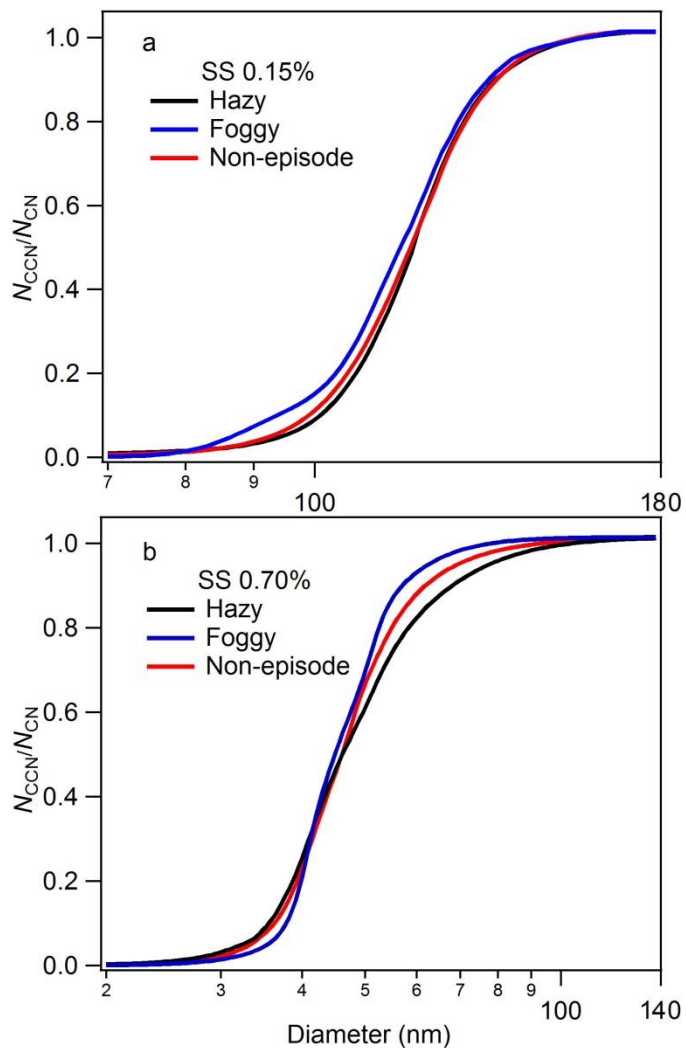
913 Fig.5. Predictions of N_{CCN} based on i (a-d) the individual D_{50} and (e-h) the average D_{50} over the
 914 whole period from κ_{AMS_B} , ii (a-d) the individual D_{50} and (e-h) the average D_{50} over the whole
 915 period from κ_{AMS_SR} and iii (a-d) the average D_{50} and (e-h) the average size-resolved CCN
 916 activation ratio from CCN measurement over the whole period.

917
918
919
920
921
922
923
924
925
926
927
928
929
930
931
932
933
934
935



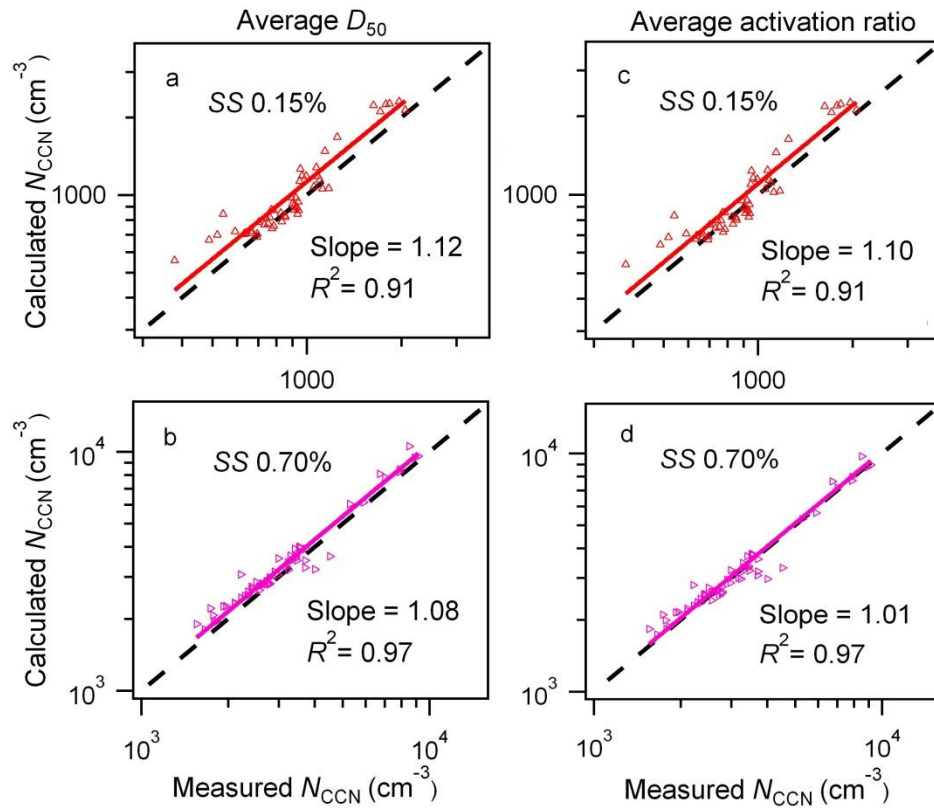
936 Fig.6. The average aerosol size distribution over the whole period (a), N_{CCN} prediction based on
937 D_{50} at SS of (b) 0.15% and (c) 0.70%. Data points are mean values and standard deviation.

938
939
940
941
942
943
944
945
946
947
948
949
950
951
952
953
954
955
956
957
958
959
960



961 Fig.7. The average size-resolved CCN activation ratio at SS of (a) 0.15% and (b) 0.70% during
962 the hazy, foggy and non-episode periods.

963
964
965
966
967
968
969
970
971
972
973
974
975
976
977
978
979
980
981
982
983
984
985



986 Fig.8. N_{CCN} estimations in the hazy period based on (a and b) the average D_{50} and (c and d) the
987 average size-resolved CCN activation ratio from CCN measurement over the hazy period.